A Local Thermal Nonequilibrium Analysis of Silicon Carbide Ceramic Foam as a Solar Volumetric Receiver

Y. Sano

S. Iwase

Department of Mechanical Engineering,
Shizuoka University,
3-5-1 Johoku, Naka-ku,
Hamamatsu 432-8561, Japan

A. Nakayama

Department of Mechanical Engineering,
Shizuoka University,
3-5-1 Johoku, Naka-ku,
Hamamatsu 432-8561, Japan;
School of Civil Engineering and Architecture,
Wuhan Polytechnic University,
Wuhan, Hubei 430023, China

A volumetric solar receiver receives the concentrated radiation generated by a large number of heliostats. Heat transfer takes place from the receiver solid phase to the air as it passes through the porous receiver. Such combined heat transfer within the receiver, associated radiation, convection and conduction, are investigated using a local thermal nonequilibrium model. The Rosseland approximation is applied to account for the radiative heat transfer through the solar receiver, while the low Mach approximation is exploited to investigate the compressible flow through the receiver. Analytic solutions are obtained for the developments of air and ceramic temperatures as well as the pressure along the flow direction. The results show that the pore diameter must be larger than its critical value to achieve high receiver efficiency. Subsequently, there exists an optimal pore diameter for achieving the maximum receiver efficiency under the equal pumping power. The solutions serve as a useful tool for designing a novel volumetric solar receiver of silicon carbide ceramic foam. [DOI: 10.1115/1.4005758]

Keywords: thermal nonequilibrium, volumetric solar receiver, porous media, ceramic foam

Introduction

Solar power technology has drawn tremendous attention in recent years, as a promising way to generate electricity from concentrated solar power. In a solar power tower plant, a volumetric receiver is the central element of the technology. It is used to receive the concentrated radiation generated by a large number of controlled mirrors (i.e., heliostats). The volumetric receiver which is made of high temperature resistant porous materials absorbs the radiation and converts it into heat. The air being sucked into the receiver is heated up, as it passes through the porous receiver. This hot air is usually fed into a conventional boiler of steam turbine, to generate electricity.

For example, the solar power tower plant of 1.5 MW built in 2009, in Julich in Germany has more than 2000 heliostats, which result in the total mirror area of more than 20,000 m^2. The concentrated radiation from these mirrors is directed toward the silicon carbide volumetric receiver which consists of 1080 high temperature receiver elements forming the receiver front surface of 20 m^2. Thus, the heat flux on the front surface of the receiver reaches up to 1 MW/m^2 [1,2].

Requirements for a volumetric receiver are the resistance to temperature as high as 1000 °C, high porosity for sufficiently large extinction volume such that the concentrated solar radiation penetrates through the receiver, high cell density to achieve large specific surface area and sufficiently high effective thermal conductivity to avoid possible thermal spots. In consideration of these requirements, ceramic foams appear to be possible candidates to replace the conventional extruded monoliths with parallel channels (i.e., honeycomb structure) in which both thermal spots [3] and flow instabilities [4] have been frequently reported.

In the monolith receiver, locally high solar flux leads to a low mass flow with high temperature, whereas locally low solar flux leads to a high mass flow with low temperature. This causes the absorber material to exceed the design temperature locally, which then leads to its destruction although the average temperature is comparatively low. Many researchers including Becker et al. [4], Fend et al. [5], and Bai [6] focused on porous ceramic foams as a promising absorber material. These problems associated with thermal spots and flow instabilities may be overcome increasing the effective thermal conductivity and fluid mixing perpendicular to the main flow direction. Strong hydrodynamic and thermal dispersion are expected to take place within ceramic foams. Thus, silicon carbide ceramic foams appear to be the most promising candidates in views of high design temperature, hydrodynamic mixing and thermal dispersion.

In this study, we shall analytically investigate complex heat transfer taking place with the silicon carbide ceramic receiver. Some analytical and numerical investigations [3–8] have been reported. However, none of them appeared to elucidate well the combined effects of compressibility, radiation, convection and conduction within the volumetric receiver on the developments of air and ceramic temperatures as well as the pressure along the flow direction. This study appears to be the first to provide the complete set of analytical solutions based on the two-energy equation model of porous media [9,10], fully accounting for the combined effects of tortuosity, thermal dispersion, compressibility, and radiative heat transfer within a ceramic foam receiver.

Volume Avereged Governing Equations

The silicon carbide ceramic foam volumetric receiver, as schematically shown in Fig. 1, may be considered as a porous medium of homogeneous structure. In the passage, the Darcian velocity shows its dependence on the transverse direction only in a small region very close to the walls. Therefore, we may neglect the boundary effects (i.e., Brinkman term).

Neuman [11] carried out a theoretical derivation of Darcy's law and concluded that application of Darcy's law to compressible fluids is justified as long as Knudsen numbers are sufficiently small

Contributed by the Solar Energy Division of ASME for publication in the JOURNAL OF SOLAR ENERGY ENGINEERING. Manuscript received August 30, 2011; final manuscript received November 16, 2011; published online February 27, 2012. Assoc. Editor: Wojciech Lipinski.

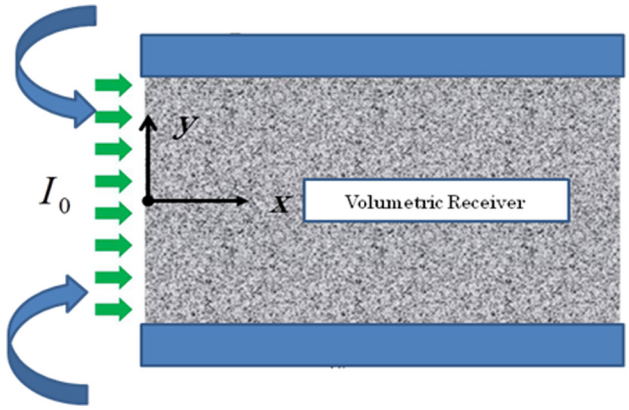

Fig. 1 Volumetric receiver

to ensure the no-slip conditions at the solid–gas interface. This is usually the case for the volumetric receivers. Thus, allowing the density to vary through the receiver, the following Forchheimer extended Darcy law should hold

$$-\frac{\partial\langle p\rangle^f}{\partial x_i}=\frac{\langle\mu\rangle^f}{K}\langle u_i\rangle+b\langle\rho\rangle^f\sqrt{\langle u_j\rangle\langle u_j\rangle}\langle u_i\rangle \tag{1}$$

where K is the permeability and b is the inertial coefficient. Furthermore, using the volume averaging procedure [12–14], the energy equation for compressible flows and that for the solid phase may be integrated over an elemental control volume V to obtain the volume average set of the macroscopic energy equations. (Note that the length scale $V^{1/3}$ is much smaller than the macroscopic characteristic length, but, at the same time, much greater than the pore diameter.) Upon assuming that the porous medium is isotropic and its porosity is uniform everywhere, the integration of the two distinct energy equations yields:

For the air

$$\begin{aligned}&\varepsilon\frac{\partial}{\partial t}\left\langle\rho_f\left(h_{stag}-\frac{p}{\rho}\right)\right\rangle^f+\varepsilon\frac{\partial}{\partial x_j}\langle\rho\rangle^f\langle u_j\rangle^f\langle h_{st}\rangle^f\\&=\frac{\partial}{\partial x_j}\left(\varepsilon\langle k_f\rangle^f\frac{\partial\langle T\rangle^f}{\partial x_j}+\frac{1}{V}\int_{A_{\text{int}}}k_fTn_jdA-\varepsilon\langle\rho\rangle^f\langle\tilde{h}_{stag}\tilde{u}_j\rangle^f+\varepsilon\langle u_i\tau_{ij}\rangle^f\right)\\&\quad+\frac{1}{V}\int_{A_{\text{int}}}k_f\frac{\partial T}{\partial x_j}n_jdA\end{aligned} \tag{2}$$

For the solid matrix

$$\begin{aligned}(1-\varepsilon)\rho_sc_s\frac{\partial\langle T\rangle^s}{\partial t}&=\frac{\partial}{\partial x_j}\left((1-\varepsilon)k_s\frac{\partial\langle T\rangle^s}{\partial x_j}-\frac{k_s}{V}\int_{A_{\text{int}}}Tn_jdA\right.\\&\quad\left.+\frac{16\sigma}{3\beta}(\langle T\rangle^s)^3\frac{\partial\langle T\rangle^s}{\partial x_j}\right)-\frac{1}{V}\int_{A_{\text{int}}}k_f\frac{\partial T}{\partial x_j}n_jdA\end{aligned} \tag{3}$$

where the volume average of a certain local variable ϕ in the fluid phase is defined as

$$\langle\phi\rangle^f\equiv\frac{1}{V_f}\int_{V_f}\phi dV \tag{4}$$

such that $\langle T\rangle^f$ is the intrinsic volume average of the fluid temperature, while $\langle T\rangle^s$ is the intrinsic volume average of the solid matrix temperature, where V_f is the volume space which the fluid phase occupies. The porosity $\varepsilon\equiv V_f/V$ is the volume fraction of the fluid space. The local variable ϕ is decomposed into its intrinsic average and the spatial deviation from it

$$\phi=\langle\phi\rangle^f+\tilde{\phi} \tag{5}$$

Moreover, A_{int} is the local interfacial area between the fluid and solid matrix, while n_j is the unit vector pointing outward from the fluid side to solid side. Note that some terms have disappeared due to the no-slip conditions while others have been replaced by the fluid phase counterparts due to the continuity of both temperature and heat flux imposed on the interface.

Since the silicon carbide ceramic foam is optically thick, we have appealed to the Rosseland approximation. Thus, we assume that radiant energy emitted from other locations in the domain is quickly absorbed and has no influence on the local transport, such that the radiative heat flux is given by

$$q_R=-\frac{16\sigma}{3\beta}(\langle T\rangle^s)^3\frac{\partial\langle T\rangle^s}{\partial x_j} \tag{6}$$

where $\sigma=5.67\times10^{-8}$ W/m^{2}K^4 is the Stephan–Boltzmann constant while β is the mean extinction coefficient. Obviously, the parenthetical terms including this radiative heat flux term on the right-hand side of Eq. (3) denote the diffusive heat transfer, while the last term describes the interfacial heat transfer between the solid and fluid phases.

Furthermore, we may also appeal to the low Mach approximation to simplify the foregoing set of the equations, since the Mach number for the air flow through a porous medium is never high. Thus, the dynamic pressure change is sufficiently small as compared to the absolute pressure prevailing over the system, such that the stagnant enthalpy is approximated by $h_{stag}=h+u_ku_k/2\cong h$. Moreover, the term $\varepsilon\langle u_i\tau_{ij}\rangle^f$ within the parentheses may be dropped. Combining the foregoing two-energy Eqs. (2) and (3), and then, noting the continuity of temperature and heat flux at the interface, we obtain the single macroscopic equation for the steady state as follows:

$$\begin{aligned}\varepsilon\frac{\partial}{\partial x_j}\langle\rho_f\rangle^f\langle u_j\rangle^f\langle h\rangle^f&=\frac{\partial}{\partial x_j}\left(\varepsilon\langle k_f\rangle^f\frac{\partial\langle T\rangle^f}{\partial x_j}+(1-\varepsilon)k_s\frac{\partial\langle T\rangle^s}{\partial x_j}\right.\\&\quad+\frac{1}{V}\int_{A_{\text{int}}}(k_f-k_s)Tn_jdA-\varepsilon\langle\rho_f\rangle^f\langle\tilde{h}\tilde{u}_j\rangle^f\\&\quad\left.+\frac{16\sigma}{3\beta}(\langle T\rangle^s)^3\frac{\partial\langle T\rangle^s}{\partial x_j}\right)\end{aligned} \tag{7}$$

For the time being, let us assume $\partial\langle T\rangle^f/\partial x_j\cong\partial\langle T\rangle^s/\partial x_j\cong\partial\langle T\rangle/\partial x_j$. Then, the equation reduces to

$$\begin{aligned}\varepsilon\frac{\partial}{\partial x_j}\langle\rho_f\rangle^f\langle u_j\rangle^f\langle h\rangle^f&=\frac{\partial}{\partial x_j}\left(\left(\varepsilon\langle k_f\rangle^f+(1-\varepsilon)k_s\right)\frac{\partial\langle T\rangle}{\partial x_j}\right.\\&\quad+\frac{1}{V}\int_{A_{\text{int}}}(k_f-k_s)Tn_jdA-\varepsilon\langle\rho_f\rangle^f\langle\tilde{h}\tilde{u}_j\rangle^f\\&\quad\left.+\frac{16\sigma}{3\beta}(\langle T\rangle^s)^3\frac{\partial\langle T\rangle}{\partial x_j}\right)\end{aligned} \tag{8}$$

where

$$\langle\phi\rangle\equiv\frac{1}{V}\int_V\phi dV \tag{9}$$

is the Darcian average of the variable ϕ such that $\langle u_j\rangle=\varepsilon\langle u_j\rangle^f$ is the Darcian velocity vector. From the foregoing Eq. (6), the

macroscopic heat flux vector $q_i = (q_x, q_y, q_z)$ and its corresponding stagnant thermal conductivity k_{stag} may be defined as follows:

$$q_i = -\left(k_{stag} + \frac{16\sigma}{3\beta}(\langle T\rangle^s)^3\right)\frac{\partial\langle T\rangle}{\partial x_i} + \varepsilon\langle\rho_f\rangle^f\langle\tilde{h}\tilde{u}_i\rangle^f$$
$$= -\left(\varepsilon\langle k_f\rangle^f + (1-\varepsilon)k_s\right)\frac{\partial\langle T\rangle}{\partial x_i} - \frac{1}{V}\int_{A_{\text{int}}}(k_f - k_s)Tn_i dA \quad (10a)$$
$$-\frac{16\sigma}{3\beta}(\langle T\rangle^s)^3\frac{\partial\langle T\rangle}{\partial x_i} + \varepsilon\langle\rho_f\rangle^f\langle\tilde{h}\tilde{u}_i\rangle^f$$

or

$$k_{stag}\frac{\partial\langle T\rangle}{\partial x_i} = \left(\varepsilon\langle k_f\rangle^f + (1-\varepsilon)k_s\right)\frac{\partial\langle T\rangle}{\partial x_i} + \frac{1}{V}\int_{A_{\text{int}}}(k_f - k_s)Tn_i dA \quad (10b)$$

The term $\varepsilon\langle\rho_f\rangle^f\langle\tilde{h}\tilde{u}_i\rangle^f$ in Eq. (10*a*) describes the thermal dispersion heat flux vector which serves an additional heat flux resulting from the hydrodynamic mixing due to the presence of obstacles. On the other hand, the second term right-hand side term in Eq. (10*b*) associated with the surface integral, describes the effects of the tortuosity on the macroscopic heat flux, which adjusts the level of the stagnant thermal conductivity from its upper bound $(\varepsilon k_f + (1-\varepsilon)k_s)$ to a correct one. Yang and Nakayama [10] introduced the effective porosity ε^* which is defined as

$$\varepsilon^* = \frac{k_s - k_{stag}}{k_s - k_f} = \varepsilon + \frac{\varepsilon k_f + (1-\varepsilon)k_s - k_{stag}}{k_s - k_f} \quad (11)$$

such that

$$(\varepsilon^* - \varepsilon)\frac{\partial\langle T\rangle}{\partial x_i} = \frac{1}{V}\int_{A_{\text{int}}} Tn_i dA \quad (12)$$

Using the effective porosity ε^* and the equation of state $\langle p\rangle^f = \langle\rho_f\rangle^f R\langle T\rangle^f$ and $\langle h\rangle^f = c_p\langle T\rangle^f$, the volume average energy Eqs. (2) and (3) may be concisely rewritten for the steady state as

For the air

$$\varepsilon c_p\frac{\partial}{\partial x_j}\langle\rho_f\rangle^f\langle u_j\rangle^f\langle T\rangle^f$$
$$= \frac{\partial}{\partial x_j}\left(\varepsilon^*\langle k_f\rangle^f\frac{\partial\langle T\rangle^f}{\partial x_j} + \varepsilon k_{\text{dis}_{jk}}\frac{\partial\langle T\rangle^f}{\partial x_k}\right) - h_v\left(\langle T\rangle^f - \langle T\rangle^s\right) \quad (13)$$

For the solid matrix phase

$$\frac{\partial}{\partial x_j}\left((1-\varepsilon^*)k_s + \frac{16\sigma}{3\beta}(\langle T\rangle^s)^3\right)\frac{\partial\langle T\rangle^s}{\partial x_j} - h_v\left(\langle T\rangle^s - \langle T\rangle^f\right) = 0 \quad (14)$$

Note that the assumption of equal temperature gradients, $\partial\langle T\rangle^f/\partial x_j \cong \partial\langle T\rangle^s/\partial x_j \cong \partial\langle T\rangle/\partial x_j$, has been discarded. This practice has been proven to be quite effective in a series of computations (e.g., Refs. [9, 10]). Moreover, the thermal dispersion term is modeled according to the gradient diffusion hypothesis [15]

$$\langle\rho_f\rangle^f\langle\tilde{h}\tilde{u}_j\rangle^f = \langle\rho_f\rangle^f c_p\langle\tilde{T}\tilde{u}_j\rangle^f = -k_{disjk}\frac{\partial\langle T\rangle^f}{\partial x_k} \quad (15)$$

while the interfacial heat transfer between the solid and fluid phases is modeled using Newton's cooling law

$$\frac{1}{V}\int_{A_{\text{int}}} k_f\frac{\partial T}{\partial x_j}n_j dA = h_v\left(\langle T\rangle^s - \langle T\rangle^f\right) \quad (16)$$

where h_v is the volumetric heat transfer coefficient. The Maxwell approximations may be used for the dynamic viscosity and thermal conductivity of the air

$$\mu\left(\langle T\rangle^f\right) = \mu_0\left(\frac{\langle T\rangle^f}{\langle T\rangle_0^f}\right)^n = 1.8\times10^{-5}\left(\frac{\langle T\rangle^f}{300\,\text{K}}\right)^{0.7}\ [\text{Pa}\cdot\text{s}] \quad (17a)$$

and

$$k_f\left(\langle T\rangle^f\right) = k_0\left(\frac{\langle T\rangle^f}{\langle T\rangle_0^f}\right)^n = 0.025\left(\frac{\langle T\rangle^f}{300\,\text{K}}\right)^{0.7}\ [\text{W/mK}] \quad (17b)$$

where the exponent n is 0.7 according to Ref. [4]. The specific heat capacity of the air $c_p = 1000\,\text{J/kgK}$ and the Prandtl number $Pr = 1.8\times10^{-5}\times1000/0.025 = 0.72$ are assumed to be constant.

One Dimensional Analysis for Volumetric Receiver

We shall seek possible analytic solutions for convective-radiative heat transfer within a receiver filled with silicon carbide ceramic foam. As illustrated in Fig. 1, the air is being sucked to flow at the rate of the mass flux $G = \langle\rho_f\rangle^f\langle u\rangle$ through a passage of length L. Under the low Mach number approximation, namely $\langle\rho_f\rangle^f \propto 1/\langle T\rangle^f$, we may reduce the macroscopic governing Eqs. (1), (13), and (14) to a one-dimensional set of the equations as follows:

$$-\frac{d\langle p\rangle^f}{dx} = \frac{\langle\mu\rangle^f}{K}\frac{G}{\langle\rho_f\rangle^f} + b\frac{G^2}{\langle\rho_f\rangle^f} = \frac{R}{\langle p\rangle^f}\left(\frac{\langle\mu\rangle^f}{K}G + bG^2\right)\langle T\rangle^f \quad (18)$$

$$c_pG\frac{d\langle T\rangle^f}{dx} = \frac{d}{dx}\left(\varepsilon^*\langle k_f\rangle^f + \varepsilon k_{disxx}\right)\frac{d\langle T\rangle^f}{dx} - h_v\left(\langle T\rangle^f - \langle T\rangle^s\right) \quad (19)$$

$$\frac{d}{dx}\left((1-\varepsilon^*)k_s + \frac{16\sigma}{3\beta}(\langle T\rangle^s)^3\right)\frac{d\langle T\rangle^s}{dx} - h_v\left(\langle T\rangle^s - \langle T\rangle^f\right) = 0 \quad (20)$$

According to Calmid and Mahajan [16,17], Dukhan [18], Kuwahara et al. [19], and Yang et al. [20,21], the permeability and inertial coefficient of foams are given by

$$K = 0.00073(1-\varepsilon)^{-0.224}\left(\frac{1.18}{1-e^{-(1-\varepsilon)/0.04}}\sqrt{\frac{1-\varepsilon}{3\pi}}\right)^{-1.11}d_m^2 \quad (21)$$

and

$$b = \frac{12(1-\varepsilon)}{d_m} \quad (22)$$

respectively, where d_m is the pore diameter of foam. The longitudinal dispersion coefficient is roughly about 20 times more than the transverse one. Thus, following Calmid and Mahajan [16], we may evaluate the longitudinal dispersion coefficient using the following expression:

$$\varepsilon k_{dis_{xx}} = 1.2c_pG\sqrt{K} \quad (23)$$

Furthermore, Calmid and Mahajan [16,17] empirically provided the stagnant thermal conductivity and the volumetric heat transfer coefficient for foams as follows:

$$k_{stag} = \varepsilon k_f + 0.19(1-\varepsilon)^{0.763}k_s \quad (24)$$

$$h_v = 8.72(1-\varepsilon)^{1/4}\left(\frac{1-e^{-(1-\varepsilon)/0.04}}{\varepsilon}\right)^{1/2}\left(\frac{Gd_m}{\langle\mu\rangle^f}\right)^{1/2} Pr^{0.37}\frac{k_f}{d_m^2} \tag{25}$$

Alternative empirical correlations for the volumetric heat transfer coefficient h_v of foams may be found elsewhere [22].

Kamiuto et al. [23] experimentally showed that the Rosseland model is quite effective and sufficiently accurate to describe radiative heat transfer within cordierite ceramic slabs. Thus, the Rosseland model is assumed to be applicable also for the present case of silicon carbide ceramic foam. The mean extinction coefficient β is assumed to be proportional to $(1-\varepsilon)/d_m$. The measurements made on cordierite ceramic foams by Kamiuto et al. give us the following correlation:

$$\beta = 8(1-\varepsilon)/d_m \tag{26}$$

For given mass flux $G = \langle\rho_f\rangle^f\langle u\rangle$, the foregoing three equations along with the equation of state may be solved for the four unknowns, namely, $\langle T\rangle^f$, $\langle T\rangle^s$, $\langle p\rangle^f$, and $\langle\rho_f\rangle^f$. The boundary conditions are given as follows:

$$x = 0 \text{ (Inlet)}$$

$$\langle T\rangle^f = \langle T\rangle_0^f = 300\,\text{K} \tag{27}$$

$$\langle p\rangle^f = \langle p\rangle_0^f = 10^5\,\text{Pa} \tag{28}$$

such that $\langle\rho_f\rangle^f = \langle\rho_f\rangle_0^f = \langle p\rangle_0^f/R\langle T\rangle_0^f = 10^5/(287\times 300) = 1.2\,\text{kg/m}^3$

$$-\left(\varepsilon^*\langle k_f\rangle^f + \varepsilon k_{disxx}\right)\frac{d\langle T\rangle^f}{dx}\bigg|_{x=0} - \left((1-\varepsilon^*)k_s + \frac{16\sigma}{3\beta}(\langle T\rangle^s)^3\right)\frac{d\langle T\rangle^s}{dx}\bigg|_{x=0}$$
$$= I_0\cos\xi - (1-\varepsilon)\left(a\sigma\left((\langle T\rangle_0^s)^4 - \left(\langle T\rangle_0^f\right)^4\right) + h_{conv}\left(\langle T\rangle_0^s - \langle T\rangle_0^f\right)\right) \tag{29}$$

where I_0 is the intensity of radiation and ξ is the incidence angle. Moreover, $a \cong 0.9$ is the emissivity of the front surface of the receiver, while h_{conv} is the convective heat transfer coefficient at the frontal surface. The properties of the air depend on the temperature, which makes the integrations of the foregoing governing equations formidable. In order to obtain analytic expressions for the unknown variables, we may approximate these properties by their representative values evaluated at the average air temperature over the receiver as given by

$$\overline{\langle T\rangle^f} = \frac{1}{L}\int_0^L \langle T\rangle^f dx \tag{30a}$$

Likewise we shall define the solid phase average temperature as follows:

$$\overline{\langle T\rangle^s} = \frac{1}{L}\int_0^L \langle T\rangle^s dx \tag{30b}$$

The errors associated with this linearization practice are quite small, as will be confirmed later by comparing these approximate results with the direct numerical integration results.

The two-energy Eqs. (19) and (20) may be added together and integrated using the boundary conditions (27) and (29) to give

$$c_pG\left(\langle T\rangle^f - \langle T\rangle_0^f\right) = \left(\varepsilon^*k_0\left(\frac{\overline{\langle T\rangle^f}}{\langle T\rangle_0^f}\right)^n + \varepsilon k_{disxx}\right)\frac{d\langle T\rangle^f}{dx} + \left((1-\varepsilon^*)k_s + \frac{16\sigma}{3\beta}\left(\overline{\langle T\rangle^s}\right)^3\right)\frac{d\langle T\rangle^s}{dx} + I_0\cos\xi - (1-\varepsilon)\left(a\sigma\left((\langle T\rangle_0^s)^4 - \left(\langle T\rangle_0^f\right)^4\right) + h_{\text{cov}}\left(\langle T\rangle_0^s - \langle T\rangle_0^f\right)\right) \tag{31}$$

This equation is substituted into Eq. (19) to eliminate $\langle T\rangle^s$ in favor of $\langle T\rangle^f$. The resulting ordinary differential equation for $\langle T\rangle^f$ runs as

$$\frac{d^3\langle T\rangle^f}{dx^3} = \frac{Gc_p}{\varepsilon^*k_0\left(\frac{\overline{\langle T\rangle^f}}{\langle T\rangle_0^f}\right)^n + \varepsilon k_{disxx}}\frac{d^2\langle T\rangle^f}{dx^2}$$
$$+h_v\frac{k_{stag}+\varepsilon k_{disxx}+\frac{16\sigma}{3\beta}\left(\overline{\langle T\rangle^s}\right)^3}{\left(\varepsilon^*k_0\left(\frac{\overline{\langle T\rangle^f}}{\langle T\rangle_0^f}\right)^n + \varepsilon k_{disxx}\right)\left((1-\varepsilon^*)k_s+\frac{16\sigma}{3\beta}\left(\overline{\langle T\rangle^s}\right)^3\right)}\frac{d\langle T\rangle^f}{dx}$$
$$-h_v\frac{Gc_p}{\left(\varepsilon^*k_0\left(\frac{\overline{\langle T\rangle^f}}{\langle T\rangle_0^f}\right)^n + \varepsilon k_{disxx}\right)\left((1-\varepsilon^*)k_s+\frac{16\sigma}{3\beta}\left(\overline{\langle T\rangle^s}\right)^3\right)}\langle T\rangle^f$$
$$+h_v\frac{I_0\cos\xi-(1-\varepsilon)\left(a\sigma\left((\langle T\rangle_0^s)^4-\left(\langle T\rangle_0^f\right)^4\right)+h_{\text{cov}}\left(\langle T\rangle_0^s-\langle T\rangle_0^f\right)\right)}{\left(\varepsilon^*k_0\left(\frac{\overline{\langle T\rangle^f}}{\langle T\rangle_0^f}\right)^n + \varepsilon k_{disxx}\right)\left((1-\varepsilon^*)k_s+\frac{16\sigma}{3\beta}\left(\overline{\langle T\rangle^s}\right)^3\right)} \tag{32}$$

This ordinary differential equation, with the boundary conditions (27)–(29) and the auxiliary asymptotic condition $d\langle T\rangle_0^f/dx = d^2\langle T\rangle_0^f/dx^2 = 0$, yields

$$\langle T\rangle^f = T_{eq} - \left(T_{eq} - \langle T\rangle_0^f\right)e^{-\gamma\lambda x} \tag{33}$$

and

$$\langle T\rangle^s = T_{eq} - \left(T_{eq} - \langle T\rangle_0^s\right)e^{-\gamma\lambda x} \tag{34}$$

where γ is the positive real root which can uniquely be determined from the following cubic equation:

$$\gamma^3 + \frac{Gc_p}{\left(\varepsilon^*k_0\left(\frac{\overline{\langle T\rangle^f}}{\langle T\rangle_0^f}\right)^n + \varepsilon k_{disxx}\right)\lambda}\gamma^2 - \gamma - \frac{Gc_p}{\left(k_{stag}+\varepsilon k_{disxx}+\frac{16\sigma}{3\beta}\left(\overline{\langle T\rangle^s}\right)^3\right)\lambda} = 0 \tag{35}$$

where

$$\lambda = \sqrt{\frac{\left(k_{stag}+\varepsilon k_{disxx}+\frac{16\sigma}{3\beta}\left(\overline{\langle T\rangle^s}\right)^3\right)h_v}{\left(\varepsilon^*k_0\left(\frac{\overline{\langle T\rangle^f}}{\langle T\rangle_0^f}\right)^n + \varepsilon k_{disxx}\right)\left((1-\varepsilon^*)k_s+\frac{16\sigma}{3\beta}\left(\overline{\langle T\rangle^s}\right)^3\right)}} \tag{36}$$

The solid phase temperature at the inlet $\langle T\rangle_0^s$ and temperature at the thermal equilibrium, namely, $T_{eq} = \langle T\rangle_\infty^f = \langle T\rangle_\infty^s$, are given by

$$\langle T\rangle_0^s = T_{eq} + \left(T_{eq} - \langle T\rangle_0^f\right)\frac{Gc_p + \left(\varepsilon^*k_0\left(\frac{\overline{\langle T\rangle^f}}{\langle T\rangle_0^f}\right)^n + \varepsilon k_{disxx}\right)\gamma\lambda}{\left((1-\varepsilon^*)k_s+\frac{16\sigma}{3\beta}\left(\overline{\langle T\rangle^s}\right)^3\right)\gamma\lambda} \tag{37}$$

and

$$T_{eq} = \langle T\rangle_0^f + \frac{I_0\cos\xi - (1-\varepsilon)\left(a\sigma\left(\left(\langle T\rangle_0^s\right)^4 - \left(\langle T\rangle_0^f\right)^4\right) + h_{\text{cov}}\left(\langle T\rangle_0^s - \langle T\rangle_0^f\right)\right)}{Gc_p} \tag{38}$$

respectively. Usually, the receiver length L is sufficiently long to reach the local thermal equilibrium. Thus, the average air and solid temperatures are evaluated from

$$\overline{\langle T\rangle^f} = \frac{1-e^{-\gamma\lambda L}}{\gamma\lambda L}\langle T\rangle_0^f + \left(1 - \frac{1-e^{-\gamma\lambda L}}{\gamma\lambda L}\right)T_{eq} \cong \frac{1}{\gamma\lambda L}\langle T\rangle_0^f + \left(1-\frac{1}{\gamma\lambda L}\right)T_{eq} \tag{39a}$$

$$\overline{\langle T\rangle^s} = \frac{1-e^{-\gamma\lambda L}}{\gamma\lambda L}\langle T\rangle_0^s + \left(1 - \frac{1-e^{-\gamma\lambda L}}{\gamma\lambda L}\right)T_{eq} \cong \frac{1}{\gamma\lambda L}\langle T\rangle_0^s + \left(1-\frac{1}{\gamma\lambda L}\right)T_{eq} \tag{39b}$$

For given inlet air temperature $\langle T\rangle_0^f$, Eqs. (37) and (38) together with Eqs. (39*a*) and (39*b*) may easily be combined iteratively to find the solid phase temperature at the inlet $\langle T\rangle_0^s$ as well as the thermal equilibrium temperature T_{eq}.

The receiver efficiency is one of the most important performance parameters, which is defined by

$$\eta = \frac{I_0\cos\xi - (1-\varepsilon)\left(a\sigma\left(\left(\langle T\rangle_0^s\right)^4 - \left(\langle T\rangle_0^f\right)^4\right) + h_{\text{cov}}\left(\langle T\rangle_0^s - \langle T\rangle_0^f\right)\right)}{I_0\cos\xi} \tag{40}$$

Having established the temperature development, the momentum Eq. (18) along with the equation of state can easily be solved to find out the pressure distribution along the receiver as

$$\langle p\rangle^f = \sqrt{\left(\langle p\rangle_0^f\right)^2 - 2R\left(\frac{\mu_0}{K}\left(\frac{\overline{\langle T\rangle^f}}{\langle T\rangle_0^f}\right)^n G + bG^2\right)\left(\frac{1-e^{-\gamma\lambda x}}{\gamma\lambda}\langle T\rangle_0^f + \left(x - \frac{1-e^{-\gamma\lambda x}}{\gamma\lambda}\right)T_{eq}\right)} \tag{41}$$

Under the low Mach approximation, the required pumping power per unit frontal area may be evaluated from

$$\begin{aligned} PP &= G\int_0^L -\frac{d\langle p\rangle^f}{\langle\rho_f\rangle^f} = G\int_0^L -\frac{1}{\langle\rho_f\rangle^f}\frac{d\langle p\rangle^f}{dx}dx \\ &= \left(\frac{R}{\langle p\rangle_0^f}\right)^2 G\left(\frac{\mu_0}{K}\left(\frac{\overline{\langle T\rangle^f}}{\langle T\rangle_0^f}\right)^n G + bG^2\right)\int_0^L \left(\langle T\rangle^f\right)^2 dx \\ &= \left(\frac{R}{\langle p\rangle_0^f}\right)^2 G\left(\frac{\mu_0}{K}\left(\frac{\overline{\langle T\rangle^f}}{\langle T\rangle_0^f}\right)^n G + bG^2\right)L \\ &\quad\times\left(T_{eq}^2 - \frac{2\left(1-e^{-\gamma\lambda L}\right)}{\gamma\lambda L}T_{eq}\left(T_{eq} - \langle T\rangle_0^f\right) + \frac{1-e^{-2\gamma\lambda L}}{2\gamma\lambda L}\left(T_{eq} - \langle T\rangle_0^f\right)^2\right) \\ &\cong \frac{G}{\left(\langle\rho\rangle_0^f\right)^2}\left(\frac{\mu_0}{K}\left(\frac{\overline{\langle T\rangle^f}}{\langle T\rangle_0^f}\right)^n G + bG^2\right)\frac{1}{2\gamma\lambda} \\ &\quad\times\left((2\gamma\lambda L - 3)\left(\frac{T_{eq}}{\langle T\rangle_0^f}\right)^2 + 2\left(\frac{T_{eq}}{\langle T\rangle_0^f}\right) + 1\right) \end{aligned} \tag{42}$$

Note that the dynamic pressure change is sufficiently small as compared to the absolute pressure such that $\langle\rho_f\rangle^f \propto 1/\langle T\rangle^f$.

Comparison With Numerical Results

Smirnova et al. [24] used the commercial software COMSOL for multiphysics modeling and simulations of compressible fluid flow and heat transfer within the solar receiver with silicon carbide monolithic honeycombs. They exploited the COMSOL application modes, in which convection, conduction and radiation can be handled, allowing the heat transfer between the solid and fluid phases. They used the homogeneous three-dimensional model, called Autodesk Inventor, to draw the volumetric receiver as a porous continuum. In order to obtain the analytic solutions based on the present local thermal nonequilibrium model, we collected the following input data from their paper:

$\langle\rho_f\rangle_0^f = 1.2\,\text{kg/m}^3$, $\langle T\rangle_0^f = 300\,\text{K}$ $(\langle p\rangle_0^f = 10^5\,\text{Pa})$, $c_p = 1000\,\text{J/kgK}$, $G = 1.2\,\text{kg/m}^2\text{s}$, $L = 0.05\,\text{m}$, $I_0 = 10^6\,\text{W/m}^2$, $\xi = 0$, $h_{conv} = 0\,\text{W/m}^2\text{K}$, $k_s = 150\,\text{W/mK}$ $k_{dis} = 0\,\text{W/m K}$, $h_v = 8.8\times10^4\,\text{W/m}^3\text{K}$, $\varepsilon = 0.5$, $\beta = 50\,1/\text{m}$

Since the porosity of the silicon carbide monolithic honeycombs is not available in Smirnova et al. [24], its value was estimated to be $\varepsilon = 0.5$ from the figure provided by Agrafiotis et al. [25]. The mean extinction coefficient β for silicon carbide monolithic honeycombs is not available in their paper. It may be much less than those of the ceramic foams, since the solar radiation penetrates through the receiver much deeper in such a monolithic receiver than in a foam receiver. Finally, the value was estimated to be 50 1/m by correlating the present results against theirs. It should also

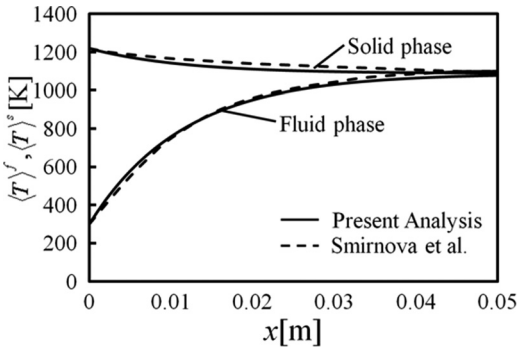

Fig. 2 Axial developments of the fluid and solid phase temperatures: Comparison of the present analysis and FEM analysis

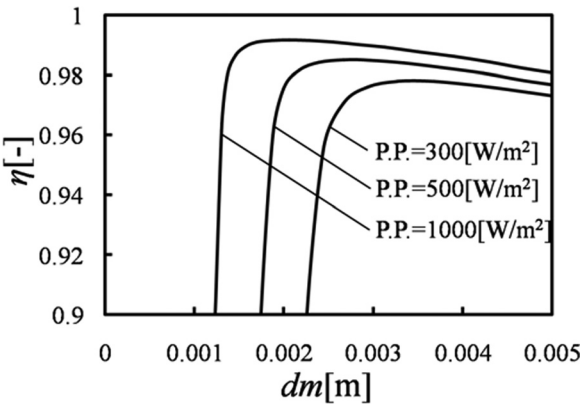

Fig. 4 Effects of the pore diameter on the receiver efficiency

be noted that the convective heat transfer coefficient was set to zero since radiation predominates over convection in the receiver front.

In Fig. 2, the present analytic solutions are compared against the large scale finite element method (FEM) numerical calculations based on COMSOL, reported by Smirnova et al. [24], in terms of the axial development of both solid and fluid temperatures. The air temperature increases as receiving heat from the monolithic receiver. The two phases reach local thermal equilibrium near the exit. Both sets of the solutions agree very well with each other, which substantiates the validity of the present local thermal nonequilibrium model. The direct numerical integrations of Eq. (18) to (20) were also carried out using the finite volume method code, SAINTS [12]. Numerical integrations were carried out using a uniform grid system, namely, 100 elements to cover the receiver. Grid refinement tests were carried out to ensure that the results are independent of grid systems. Convergence was measured in terms of the maximum change in temperature during an iteration, which was set to 10^{-5}. The numerical results thus obtained are compared against the analytical expressions (27) and (28). The difference in the two sets of curves was found indiscernible, which indicates that the linearization practice based on the average temperatures is quite effective and valid.

Applications to Silicon Carbide Ceramic Foam Volumetric Receiver

Having established the analytical expressions for pressure and temperature fields within a solar volumetric receiver, we shall investigate flow and heat transfer in silicon carbide ceramic foams, which can overcome the problems associated with thermal spots and flow instabilities. Both high thermal conductivity and fluid mixing perpendicular to the main flow direction are considered to be advantageous to avoid such thermal spots and flow instabilities.

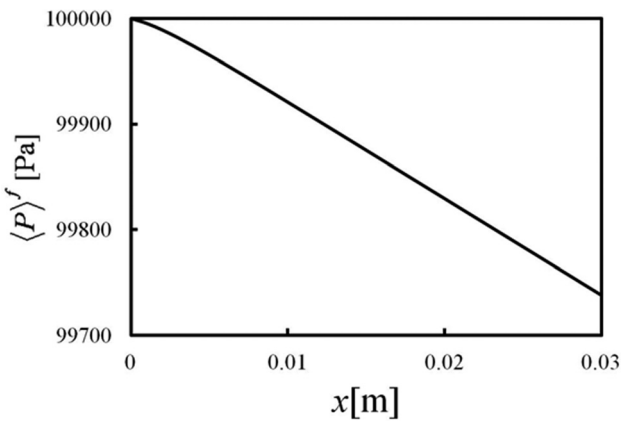

Fig. 3 Pressure distribution

A typical pressure distribution within a ceramic foam receiver is presented in Fig. 3 for the case of $G = 2.16\,\mathrm{kg/m^2s}$, $\varepsilon = 0.9$ and $d_m = 0.0021$ m. As the flow acceleration takes place at the inlet region as result of high fluid temperature, the pressure drops nonlinearly.

The performance of the receiver may be assessed in terms of the receiver efficiency η under equal pumping power PP. Thus, the effects of the pore diameter d_m on the receiver efficiency η are presented in Fig. 4. The pore diameter d_m is varied whereas the other parameters are fixed as follows:

$\langle \rho_f \rangle_0^f = 1.2\,\mathrm{kg/m^3}$, $\langle T\rangle_0^f = 300\,\mathrm{K}$ $(\langle p\rangle_0^f = 10^5\,\mathrm{Pa})$, $c_p = 1000\,\mathrm{J/kgK}$, $L = 0.03\,\mathrm{m}$, $I_0 = 10^6\,\mathrm{W/m^2}$, $\xi = 0$, $h_{conv} = 0\,\mathrm{W/m^2K}$, $k_s = 150\,\mathrm{W/mK}$, $\varepsilon = 0.9$

All other parameters are evaluated using Eqs. (17*a*) and (17*b*) and from Eqs. (21)–(26).

The figure shows a sudden rise in η at some critical value of d_m for a given value of PP, indicating that the pore diameter d_m must be larger than this critical value to achieve high η. The higher PP is, the lower the critical pore diameter is. This fact, which needs be considered as designing a volumetric receiver, can be explained in what follows.

Since $G \propto \sqrt{PP}$ for low PP and $G \propto \sqrt[3]{PP}$ for high PP as indicated by Eq. (42), the amount of heat carried by the air, $G\left(T_{eq} - \langle T\rangle_0^f\right) \propto \sqrt{PP}$, increases drastically as increasing the pumping power PP from zero. However, its rate of increase diminishes for the higher PP range, in which $G\left(T_{eq} - \langle T\rangle_0^f\right) \propto \sqrt[3]{PP}$. This change in the heat transfer rate reflects faithfully on the receiver efficiency η as can be seen from Fig. 4. The abrupt increase in the receiver efficiency takes place around the transition from the Darcy to Forchheimer regime, namely:

$$\frac{\mu_0}{K}\left(\frac{T_{eq}}{\langle T\rangle_0^f}\right)^n G_{tr} \cong bG_{tr}^2 \tag{43}$$

or

$$G_{tr} \cong \left(\frac{\mu_0}{bK}\left(\frac{I_0\cos\xi}{c_p\langle T\rangle_0^f}\right)^n\right)^{\frac{1}{1+n}} \tag{44}$$

since

$$\frac{T_{eq}}{\langle T\rangle_0^f} \cong \frac{c_pG_{tr}\langle T\rangle_0^f + I_0\cos\xi}{c_pG_{tr}\langle T\rangle_0^f} \cong \frac{I_0\cos\xi}{c_pG_{tr}\langle T\rangle_0^f} \tag{45}$$

Thus, Eq. (42) may be written for the case in which the abrupt increase in η takes place as follows:

$$PP = \frac{G_{tr}}{\left(\langle\rho\rangle_0^f\right)^2}\left(2bG_{tr}^2\right)\left(\frac{T_{eq}}{\langle T\rangle_0^f}\right)^2 L$$

$$\cong \frac{2bLG_{tr}^3}{\left(\langle\rho\rangle_0^f\right)^2}\left(\frac{I_0\cos\xi}{c_pG_{tr}\langle T\rangle_0^f}\right)^2$$

$$= \frac{2bL}{\left(\langle\rho\rangle_0^f\right)^2}\left(\frac{I_0\cos\xi}{c_p\langle T\rangle_0^f}\right)^2\left(\frac{\mu_0}{bK}\left(\frac{I_0\cos\xi}{c_p\langle T\rangle_0^f}\right)^n\right)^{\frac{1}{1+n}} \quad (46)$$

which, for given PP, gives the minimum value of the pore diameter d_{mtr}:

$$\frac{d_{mtr}}{L} = f(\varepsilon)\left(\frac{2}{\left(\langle\rho\rangle_0^f\right)^2 PP}\left(\frac{I_0\cos\xi}{c_p\langle T\rangle_0^f}\right)^3\right)^{\frac{1+n}{2+n}}\left(\frac{\mu_0}{\left(\frac{I_0\cos\xi}{c_p\langle T\rangle_0^f}\right)L}\right)^{\frac{1}{2+n}} \quad (47)$$

where

$$f(\varepsilon) = \left(\frac{(bd_m)^n}{K/d_m^2}\right)^{\frac{1}{2+n}}$$

$$= \left(\frac{(12(1-\varepsilon))^n}{0.00073(1-\varepsilon)^{-0.224}\left(\frac{1.18}{1-e^{-(1-\varepsilon)/0.04}}\sqrt{\frac{1-\varepsilon}{3\pi}}\right)^{-1.11}}\right)^{\frac{1}{2+n}} \quad (48)$$

In the case treated here, Eq. (47) gives $d_{mtr} = 0.0022$, 0.0016, and 0.0010 m for $PP = 300$, 500, and 1000 W/m^2, respectively, which is consistent with what is observed in Fig. 5. An increase in d_m (i.e., decrease in β) from d_{mtr} makes further penetration of the solar radiation possible. This works to keep the solid temperature at the inlet comparatively low such that heat loss to the ambient by radiation is suppressed. As a result, high receiver efficiency can be achieved. However, the increase in d_m on the other hand results in decreasing the volumetric heat transfer coefficient, as can be seen from Eq. (25). Too large d_m deteriorates interstitial heat transfer from the solid to air. Thus, as can be seen from the figure, the optimal size of d_m exits under the equal pumping power constraint.

In the present analysis, it is assumed that the length of the receiver is sufficiently long for the two phases to achieve local thermal equilibrium within the receiver. It is obvious that shorter length is better in view of minimizing the required pumping power, as clearly seen from Eq. (42). Thus, a minimum length required to achieve local thermal equilibrium may be chosen to design a receiver, which would guarantee both maximum receiver efficiency and minimum pumping power. Therefore, we may roughly set the optimal receiver length as

$$L = \frac{3}{\gamma\lambda} \quad (49)$$

such that

$$\frac{\langle T\rangle^f|_{x=L} - T_{eq}}{\langle T\rangle_0^f - T_{eq}} = \frac{\langle T\rangle^s|_{x=L} - T_{eq}}{\langle T\rangle_0^s - T_{eq}} = e^{-3} \cong 5\% \quad (50)$$

Equation (49) together with Eq. (47) provides useful information for designing a volumetric solar receiver of silicon carbide ceramic foam.

Conclusions

For the first time, the complete set of analytical solutions based on the two-energy equation model of porous media is presented, so as to fully account for the combined effects of tortuosity, thermal dispersion, compressibility on the convective, conductive, and radiative heat transfer within a ceramic foam receiver. The Rosseland approximation is applied to account for the radiative heat transfer through the solar receiver, while the low Mach approximation is exploited to investigate the compressible flow through the receiver. The analytic solutions are found to agree well with the large scale FEM solutions, substantiating the validity of the present solutions. Silicon carbide ceramic foams are considered as a possible candidate for the receiver which can overcome the problems associated with thermal spots and flow instabilities. The results show that the pore diameter must be larger than its critical value to achieve high receiver efficiency. As a result, there exists an optimal pore diameter for achieving the maximum receiver efficiency under the equal pumping power. The optimal pore diameter yielding the maximum receiver efficiency may be found around the critical value given by Eq. (47). A simple relation is derived for determining the length of the volumetric solar receivers of silicon carbide ceramic foam.

Acknowledgment

The authors are grateful to the late Professor K. Kamiuto (formerly Professor of Oita University) who accomplished great work on cellular porous media, for providing radiation data and stimulating our idea on this study.

Nomenclature

A = surface area (m^2)
A_{int} = interface between the fluid and solid (m^2)
b = inertial coefficient (1/m)
c = specific heat (J/kg K)
c_p = specific heat at constant pressure (J/kg K)
d_m = pore diameter (m)
G = mass flux (kg/m^2 s)
h = specific enthalpy (J/kg)
h_v = volumetric heat transfer coefficient (W/m^3 K)
I_0 = intensity of radiation (W/m^2)
k = thermal conductivity (W/m K)
K = permeability (m^2)
L = receiver length (m)
n_j = unit vector pointing outward from the fluid side to solid side (-)
PP = pumping power per unit frontal area (W/m^2)
Pr = Prandtl number (-)
q = heat flux (W/m^2)
R = gas constant (J/kg K)
T = temperature (K)
u_i = velocity vector (m/s)
V = representative elementary volume (m^3)
x_i = Cartesian coordinates (m)
x = axial coordinate (m)
β = mean extinction coefficient (1/m)
γ = dimensionless parameter (-)
ε = porosity (-)
ε^* = effective porosity (-)
ξ = incidence angle (rad)
η = receiver efficiency (-)
λ = characteristic coefficient (1/m)
μ = viscosity (Pa s)
ν = kinematic viscosity (m^2/s)
ρ = density (kg/m^2)
σ = Stephan–Boltzmann constant (W/m^2 K^4)
τ_{ij} = stress tensor (Pa)

Special Symbols

$\tilde{\phi}$ = deviation from intrinsic average
$\langle\phi\rangle$ = Darician average
$\langle\phi\rangle^{f,s}$ = intrinsic average

Subscripts and Superscripts

disp = dispersion
eq = equilibrium
f = luid
s = solid
stag = stagnation
0 = reference

References

[1] Fend, T., 2010, "High Porosity Materials as Volumetric Receivers for Solar Energetics," Opt. Appl., **11**(2), pp. 271–284.
[2] Alexopoulos, S., and Hoffschmidt, B., 2010, "Solar Tower Power Plant in Germany and Future Perspectives of the Development of the Technology in Greece and Cyprus," Renewable Energy, **35**, pp. 1352–1356.
[3] Pitz-Paal, R., Hoffschmidt, B., Bohmer, M., and Becker, M., 1997, "Experimental and Numerical Evaluation of the Performance and Flow Stability of Different Types of Open Volumetric Absorbers Under Non-Homogeneous Irradiation," Sol. Energy, **60**, pp. 135–150.
[4] Becker, M., Fend, T., Hoffschmidt, B., Pitz-Paal, R., Reutter, O., Stamatov, V., Steven, M., and Trimis, D., 2006, "Theoretical and Numerical Investigation of Flow Stability in Porous Materials Applied as Volumetric Solar Receiver," Sol. Energy, **80**, pp. 1241–1248.
[5] Fend, T., Hoffschmidt, B., Pitz-Paal, R., and Reutter, O., 2004, "Porous Materials as Open Volumetric Solar Receivers: Experimental Determination of Thermophysical and Heat Transfer Properties," Energy, **29**, pp. 823–833.
[6] Bai, F., 2010, "One Dimensional Thermal Analysis of Silicon Carbide Ceramic Foam Used for Solar Air Receiver," Int. J. Therm. Sci., **49**, pp. 2400–2404.
[7] Wu, Z., Caliot, C., Flamant, G., and Wang, Z., 2011, "Numerical Simulation of Convective Heat Transfer Between Air Flow and Ceramic Foams to Optimize Volumetric Solar Air Receiver Performances," Int. J. Heat Mass Transfer, **54**, pp. 1527–1537.
[8] Wu, Z., Caliot, C., Flamant, G., and Wang, Z., 2011, "Coupled Radiation and Flow Modeling in Ceramic Foam Volumetric Solar Air Receivers," Sol. Energy, **85**, pp. 2374–2385.
[9] Nakayama, A., Kuwahara, F., Sugiyama, M., and Xu, G. L., 2001, "A Two-Enegy Equation Model for Conduction and Convection in Porous Media," Int. J. Heat Mass Transfer, **44**, pp. 4375–4379.
[10] Yang, C., and Nakayama, A., 2010, "A Synthesis of Tortuosity and Dispersion in Effective Thermal Conductivity of Porous Media," Int. J. Heat Mass Transfer, **53**(15–16), pp. 3222–3230.
[11] Neuman, S. P., 1977, "Theoretical Derivation of Darcy's Law," Acta Mech., **25**, pp. 153–170.
[12] Cheng, P., 1978, "Heat Transfer in Geothermal Systems," Adv. Heat Transfer, **14**, pp. 1–105.
[13] Nakayama, A., 1995, *PC-Aided Numerical Heat Transfer and Convective Flow*, CRC Press, Boca Raton, pp. 103–115.
[14] Quintard, M., and Whitaker, S., 1993, "One and Two Equation Models for Transient Diffusion Processes in Two-Phase Systems," Adv. Heat Transfer, **23**, pp. 369–465.
[15] Nakayama, A., Kuwahara, F., and Kodama, Y., 2006, "An Equation for Thermal Dispersion Flux Transport and its Mathematical Modelling for Heat and Fluid Flow in a Porous Medium," J. Fluid Mech., **563**, pp. 81–96.
[16] Calmidi, V. V., and Mahajan, R. L., 1999, "The Effective Thermal Conductivity of High Porosity Fibrous Metal Foams," ASME Trans. J. Heat Transfer, **121**, pp. 466–471.
[17] Calmidi, V. V., and Mahajan, R. L., 2000, "Forced Convection in High Porosity Metal Foams," ASME Trans. J. Heat Transfer, **122**, pp. 557–565.
[18] Dukhan, N., 2006, "Correlations for the Pressure Drop for Flow Through Metal Foam," Exp. Fluids, **41**, pp. 665–672.
[19] Kuwahara, F., Yang, C., Ando, K., and Nakayama, A., 2011, "Exact Solutions for a Thermal Non-Equilibrium Model of Fluid Saturated Porous Media Based on an Effective Porosity," ASME J. Heat Transfer, **133**(11), p. 112602.
[20] Yang, C., Ando, K., and Nakayama, A., 2011, "A Local Thermal Non-Equilibrium Analysis of Fully Developed Forced Convective Flow in a Tube Filled With a Porous Medium," Transp. Porous Media, **89**, pp. 237–249.
[21] Yang, C., Kuwahara, F., Liu, W., and Nakayama, A., 2011, "Thermal Non-Equilibrium Forced Convective Flow in an Annulus Filled With a Porous Medium," Open Transp. Phenom. J., **3**, pp. 31–39.
[22] Nakayama, A., Ando, K., and Yang, C., 2009, "A Study on Interstitial Heat Transfer in Consolidated and Unconsolidated Porous Media," Heat Mass Transfer, **45**, pp. 1365–1372.
[23] Kamiuto, K., Miyoshi, Y., Kinoshita, I., and Hasegawa, S., 1983, "Conduction in Optically Thick Ceramic Porous Media: Radiative Heat Transfer for the Case of Cordierite Foam," JSME Trans., Ser. B, **49**, pp. 2147–2153.
[24] Smirnova, O., Fend, T., Schwarzbözl P., and Schollgen, D., 2010, "Homogeneous and Inhomogeneous Model for Flow and Heat Transfer in Porous Materials as High Temperature Solar Air Receiver," *Proceedings of the* COMSOL *Conference*, Paris, pp. 17–19.
[25] Agrafiotis, C., Mavroidis, I., Konstandopoulos, A. G., Hoffschmidt, B., Stobbe, P., Romero, M., and Fernandez-Quero, V., 2007, "Evaluation of Porous Silicon Carbide Monolithic Honeycombs as Volumetric Receivers/Collectors of Concentrated Solar Radiation," Sol. Energy Mater. Sol. Cells, **91**, pp. 474–488.